Proteopathic tau seeding predicts tauopathy in vivo

Brandon B. Holmes[a,1], Jennifer L. Furman[a,1], Thomas E. Mahan[a], Tritia R. Yamasaki[a], Hilda Mirbaha[a], William C. Eades[b], Larisa Belaygorod[a], Nigel J. Cairns[a], David M. Holtzman[a], and Marc I. Diamond[a,2,3]

[a]Department of Neurology, Hope Center for Neurological Disorders, Knight Alzheimer's Disease Research Center, and [b]Division of Oncology, Section of Stem Cell Biology, Department of Internal Medicine, Washington University School of Medicine, St. Louis, MO 63110

Transcellular propagation of protein aggregates, or proteopathic seeds, may drive the progression of neurodegenerative diseases in a prion-like manner. In tauopathies such as Alzheimer's disease, this model predicts that tau seeds propagate pathology through the brain via cell–cell transfer in neural networks. The critical role of tau seeding activity is untested, however. It is unknown whether seeding anticipates and correlates with subsequent development of pathology as predicted for a causal agent. One major limitation has been the lack of a robust assay to measure proteopathic seeding activity in biological specimens. We engineered an ultrasensitive, specific, and facile FRET-based flow cytometry biosensor assay based on expression of tau or synuclein fusions to CFP and YFP, and confirmed its sensitivity and specificity to tau (~300 fM) and synuclein (~300 pM) fibrils. This assay readily discriminates Alzheimer's disease vs. Huntington's disease and aged control brains. We then carried out a detailed time-course study in P301S tauopathy mice, comparing seeding activity versus histological markers of tau pathology, including MC1, AT8, PG5, and Thioflavin S. We detected robust seeding activity at 1.5 mo, >1 mo before the earliest histopathological stain. Proteopathic tau seeding is thus an early and robust marker of tauopathy, suggesting a proximal role for tau seeds in neurodegeneration.

amyloid | neuropathology | dementia | aging

Protein aggregation characterizes many neurodegenerative disorders, including Alzheimer's disease (AD) and the related tauopathies. These disorders feature the accumulation of fibrillar deposits of the microtubule-associated protein tau with progressive deterioration of the central nervous system. Tau pathology and its associated brain atrophy do not appear randomly throughout the brain, but rather progress along distinct neural networks (1–5). This aspect suggests a role for transcellular spread of a pathogenic agent via neural connections. Our laboratory and others have previously hypothesized that tau aggregates—or seeds—serve as this agent of spread, transmitting the aggregated state from cell to cell via prion-like mechanisms (6–15).

Mounting fundamental insights support this hypothesis. Tau seeds applied to the outside of cells bind the cell surface by attaching to heparan sulfate proteoglycans, triggering uptake by macropinocytosis (13). Upon internalization, tau seeds nucleate the fibrillization of endogenous tau monomer via templated conformational change, or seeding (8, 10). Tau seeding requires a critical unit of size for activity, as only particular species propagate the aggregated state (16). In vivo studies have described tau protein spreading from local sites to distant regions, presumably via transsynaptic movement (11, 12, 17–19). Finally, our laboratory and another recently demonstrated that tau propagates discrete amyloid conformations through the brains of animals that give rise to unique neuropathologies (18, 20).

Despite this evidence, it remains unclear whether the development of proteopathic tau seeding represents a causal process of tauopathy, a downstream consequence of tau fibril accumulation, a coincident trait of neurodegeneration, or even an epiphenomenon. If proteopathic seeds are indeed a causal agent of disease, then their activity should exist in the brains of tauopathy

mouse models and human subjects, precede other forms of pathology, and correlate with disease progression.

To test these hypotheses, we created a highly sensitive and quantitative assay using a novel FRET-based biosensor cell line that specifically reports tau seeding activity. With this assay, we profiled the temporal evolution of tau seeding activity in the brains of P301S transgenic mice, a model of human tauopathy, and compared it to standard measurements of histopathology taken from the same animals. We find that tau seeding marks incipient tauopathy, occurring far before the onset of several standard histopathological markers. This finding implicates proteopathic tau seeding as a proximal cause of neurodegeneration, and establishes a highly quantitative and sensitive seed detection method.

Results

FRET Flow Cytometry Quantifies Seeding Activity with High Sensitivity. Our laboratory has previously used FRET to quantify protein aggregation in cultured cells (13, 21, 22). The use of a plate reader for measuring FRET has certain disadvantages, and thus we created a facile, next-generation system to detect seeding activity with ultrahigh sensitivity and specificity. We engineered a monoclonal FRET biosensor HEK293T cell line to stably express the tau repeat domain (RD) with the disease-associated P301S mutation fused to either CFP or YFP (23, 24), hereafter, referred to as "tau biosensor cells." This line was selected for its optimized RD-CFP/YFP expression levels and minimal background FRET signal. Although at baseline the tau reporter

Significance

Prion-like propagation of proteopathic seeds may underlie the progression of neurodegenerative diseases, including the tauopathies and synucleinopathies. We aimed to construct a versatile and simple cell assay to sensitively and specifically detect proteopathic seeding activity. Using a combination of FRET flow cytometry and a tau monoclonal FRET biosensor cell line, we report seed detection in the femtomolar range. This assay is easily applied to human brain homogenates and selectively responds to Alzheimer's disease but not Huntington's disease brains. By comparing seeding activity in a mouse model of human tauopathy, we demonstrate detection of proteopathic seeding far in advance of standard histopathological markers. Proteopathic seeding is thus an early marker of tauopathy, consistent with a causal role for tau seeds in neurodegeneration.

proteins exist in a stable, soluble form within the cell, exposure to exogenous tau seeds leads to tau reporter protein aggregation, which generates a FRET signal. Mixing tau seeds with phospholipids (Lipofectamine 2000) before treating cells facilitates direct transduction of seeds into the biosensor cell line, thereby maximizing seed detection efficiency. The applied seeds nucleate aggregation of the tau FRET reporter proteins, which we detect by flow cytometry (Fig. 1A).

To validate this system, we transduced 1 nM of unlabeled, recombinant wild-type tau RD fibrils into the biosensor cells and imaged them via confocal microscopy after 24 h. At this concentration, the majority of cells converted to the aggregated state, displaying both punctate and reticular intracellular inclusions. Importantly, cells treated with empty liposomes (vehicle) never converted to an inclusion-positive state (Fig. 1B). To quantify the amount of seeded aggregation, we developed a flow cytometry-based FRET measurement algorithm similar to that described previously (25). The FRET signal, termed integrated FRET density, is calculated as the product of the percentage of FRET-positive cells and the FRET median fluorescence intensity for all cells that fall within the FRET-positive gate (Fig. S1 A and B). To determine the dynamic range and sensitivity, we transduced tau RD fibrils into the biosensor line over a wide range of concentrations (100 fM–1 μM, monomer equivalent). The FRET signal increased dose-dependently, reached statistical significance at 316 fM, and responded quantitatively over greater than three orders-of-magnitude (Fig. 1C and Fig. S1B). At 10 pM tau seeds,

the Z' score was 0.64, indicating a highly robust assay at even low seed concentrations (Fig. 1C).

To determine if the biosensor cells selectively respond to tau oligomers versus monomer, we used size-exclusion chromatography to isolate full-length monomeric tau containing two point mutations changing cysteine at 291 and 322 to alanine (tau C→A). Preventing disulfide linkage reduces spontaneous aggregation of tau monomer in vitro, enabling isolation of stable tau monomer (26). Tau C→A monomer (50 kD) as well as high molecular-weight tau oligomer fractions (~500 kDa) were purified by size-exclusion chromatography and transduced into the biosensor cells. The high molecular-weight fractions induced aggregation, but monomer did not. Thus, the assay selectively responds to pathogenic tau aggregates (Fig. S1C).

To confirm that the cellular FRET signal reliably tracks protein aggregation in the biosensor cell line, we used FACS to separate FRET-positive and FRET-negative cell populations following transduction with 500 pM tau seeds. We replated sorted cells on chambered coverslips and imaged via microscopy for the presence of intracellular inclusions. At the gate settings used, we observed ~97% sensitivity and ~93% specificity (Fig. S1D), indicating that the FRET signal reliably identifies inclusion-positive and -negative cells.

We next determined if the FRET flow cytometry assay could be used to detect α-synuclein seeding activity. Synucleinopathies, such as Parkinson's disease, feature accumulation of α-synuclein amyloids, which, like tau, may spread through the brain via prion-like mechanisms (27–31). We engineered a FRET monoclonal
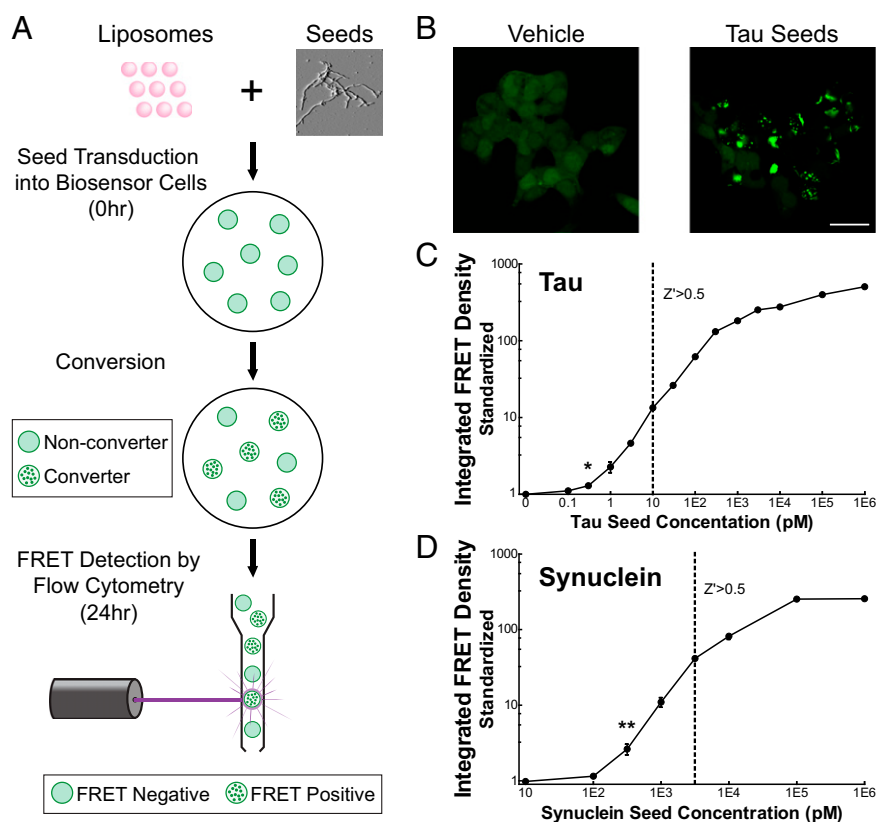

Fig. 1. FRET flow cytometry reliably detects tau seeding. (A) Schematic model of the FRET assay workflow. Lipofectamine/seed formulations are applied to biosensor cells for 24 h. Seeded aggregation produces a FRET signal that is measured by flow cytometry. (B) Confocal microscopy of tau biosensor cells transduced with liposome vehicle or tau seeds (1 nM). Tau seed-treated cells exhibit intracellular tau inclusions. (Scale bar, 20 μm.) (C) Recombinant tau RD seeds produce a dose-dependent FRET signal in the tau biosensor cells as measured by flow cytometry. (D) Recombinant α-synuclein seeds produce a dose-dependent FRET signal in the synuclein biosensor cells. Error bars show SEM; *P < 0.05; **P < 0.01; Student t test. The dashed line designates the concentration at which the Z' score exceeds 0.5.

cell line expressing full-length α-synuclein containing the disease-associated A53T mutation fused to either CFP or YFP (32). Similar to tau, we observed a robust and dose-dependent increase in FRET following transduction with wild-type α-synuclein fibrils (Fig. 1D). We conclude that the FRET-based detection system is compatible with multiple proteopathic seeds.

The FRET Seeding Assay Is Specific to Homotypic Interactions. Our laboratory previously demonstrated that template-based seeding requires homotypic interactions between seed and substrate (20), consistent with the existence of seeding barriers (33). To test the specificity of our assay, we conducted cross-seeding experiments with the tau biosensor line and measured FRET responses. Tau biosensor cells were transduced with tau RD, α-synuclein, or

Fig. 2. The tau biosensor cells are specific to tau seeds and homotypic interactions. (A) Cross-seeding experiments demonstrate that tau seeds alone produce a FRET response. Tau biosensor cells were separately transduced with 500 nM each of tau, synuclein, or Htt seeds for 24 h. Veh designates lipofectamine-only control. (B and C) Only homotypic biosensors score positive for FRET. Cells transiently transfected with tau-CFP/tau-YFP; synuclein-CFP/synuclein-YFP; or synuclein-CFP/tau-YFP were cotransduced with either 100 nM tau seeds + 100 nM synuclein seeds or lipofectamine alone. Confocal microscopy images show seed-treated heterotypic FRET biosensors (synuclein-CFP/tau-YFP). Arrows point to aggregates comprised of a single biosensor protein, either tau or synuclein; arrowhead points to an aggregate comprised of both tau and synuclein biosensors (B). (Scale bar, 10 μM.) Although all three biosensor cell lines displayed robust aggregation, FRET was only observed in the homotypic biosensor lines (C).

huntingtin (Q50) fibrils. As expected, tau RD fibrils seeded efficiently, producing a large FRET response. However, neither the synuclein nor huntingtin fibrils seeded intracellular aggregation (Fig. 2A). Thus, the tau biosensor cell line responds specifically to tau amyloids, and not to others (20, 33).

Finally, we excluded the possibility that FRET measurement is confounded by changes in fluorescence steady state (i.e., alterations in protein turnover, fluorescence pulse-width, or autofluorescence) by constructing and testing seeding in three separate biosensor cell lines: tau-CFP/tau-YFP (homotypic), synuclein-CFP/synuclein-YFP (homotypic), and synuclein-CFP/tau-YFP (heterotypic). We cotransduced these cells simultaneously with tau RD and α-synuclein fibrils, which robustly induced aggregation of both tau and synuclein in all three biosensors, as detected by confocal microscopy (Fig. 2B). However, we only detected FRET in the homotypic biosensor lines, not in the heterotypic line (Fig. 2C). Notably, FRET was undetectable in the heterotypic biosensor line even though ~25% of intracellular tau inclusions colocalized with synuclein inclusions (Fig. 2B). Thus, colocalization of different aggregates does not indicate amyloid coassembly, because only homotypic protein aggregates assemble in sufficiently tight approximation to produce a FRET response. Furthermore, because only homotypic protein aggregation produced FRET, it is unlikely that false-positive signal occurs because of alterations in fluorescent protein steady state secondary to aggregation.

FRET Flow Cytometry Detects Seeding in Primary Cultured Neurons. To assess seeding induction in more relevant neural cells and without facilitation of aggregate uptake, we tested whether FRET reliably measures tau seeding in primary neuronal cultures. We treated primary hippocampal neurons with lentivirus encoding tau RD P301S-CFP and tau RD P301S-YFP. Four days later, we exposed the neurons to tau RD fibrils without lipofectamine. Seventy-two hours after fibril treatment, neurons exhibited clear intracellular tau inclusions (Fig. 3A) that we easily measured by FRET flow cytometry (Fig. 3B and Fig. S2A). This same neuronal system also detects α-synuclein seeding activity (Fig. S2 B and C). Therefore, this assay has potentially wide applicability across culture systems.

Tau Seeding Activity Is Detected in AD Brain. Several reports have implicated prion-like seeding as a key mechanism for driving tauopathy disease progression (8, 9, 18, 34, 35). We tested the specificity of the seeding assay with human specimens chosen for a high neuropathology burden of either tau (AD parietal lobe, n = 5) or expanded huntingtin [Huntington's disease (HD) basal ganglia, n = 3] and included age-matched control brains (n = 2). AD brain lysates induced tau aggregation in the tau biosensor cells, whereas HD and control (Ct) lysates did not (Fig. 4A). Confocal microscopy confirmed these seeding results, as cells transduced with AD material displayed prominent intracellular inclusions (Fig. 4B), whereas cells treated with HD and Ct lysates lacked aggregates (Fig. 4C). These experiments further demonstrate that the bioassay selectively responds to pathogenic tau (AD) and not normal tau species (HD and Ct). Finally, to confirm that tau is necessary for seeding, we immunodepleted AD brain lysate. Lysate depletion with an anti-tau antibody (HJ8.5) substantially reduced seeding activity, whereas an anti-Aβ antibody (HJ3.4) did not (Fig. 4D). Taken together, these results indicate that the biosensor assay specifically detects pathological tau seeding in AD brain.

Seeding Activity in the P301S Tauopathy Mouse Model Increases with Age. The prion model predicts that seeding activity in diseased brains will correlate with disease progression (36, 37). To test this hypothesis, we measured seeding activity in the brains of P301S transgenic mice, a model of human tauopathy, at specific stages of disease progression (38). This well-characterized mouse model features critical hallmarks of tauopathy, including neurofibrillary tangles, tau hyperphosphorylation, synapse and neu-
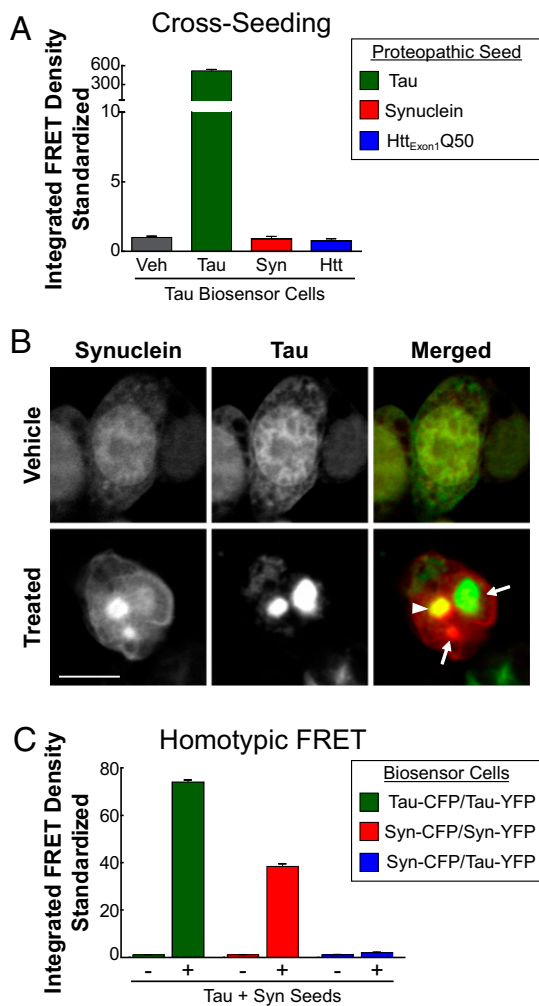
www.manaraa.com
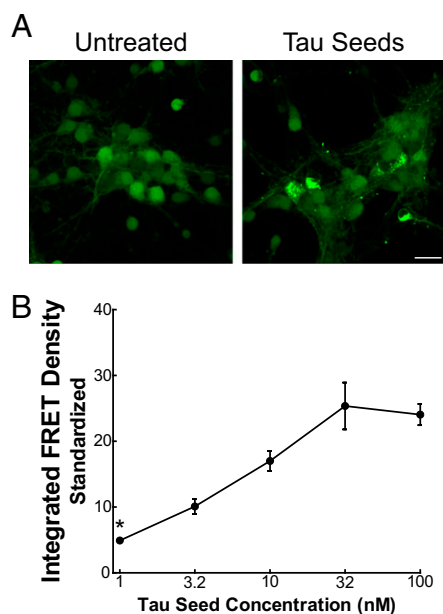
A

Untreated   Tau Seeds

B

Fig. 3. FRET flow cytometry detects physiological tau seeding in primary neurons. (*A*) Cultured mouse hippocampal neurons were transduced with lentivirus encoding tau P301S-CFP and tau P301S-YFP on day in vitro 0 and treated with 100 nM recombinant tau seeds in the absence of lipofectamine on day in vitro 4. Seventy-two hours later, neurons were imaged via confocal microscopy. (Scale bar, 20 μm.) (*B*) In the absence of lipofectamine, recombinant tau RD seeds produce a dose-dependent FRET signal in the lenti-expressing neurons as measured by FRET flow cytometry: 10,000 neurons per replicated well were analyzed; $n = 4$. Error bars show SEM; $*P < 0.0001$; Student t test.

ron loss, gliosis, altered tau levels in brain interstitial fluid and cerebrospinal fluid, and cognitive impairment (38–40). We collected P301S mouse brains, aged 1–12 mo, and microdissected the brainstem, neocortex, frontal lobe, and hippocampus from the right hemisphere. Each region was independently homogenized, and clarified lysates were transduced into the tau biosensor cell line. After 24 h, we measured seeding activity for each brain region. We detected strong seeding activity from the P301S brain homogenates, whereas aged tau knockout mice (>12 mo) never elicited a seeding response. Seeding activity became evident at 1.5 mo and increased over time in all regions (Fig. 5 and Fig. S3*A*) before saturating at near 9 mo in most animals. To exclude the possibility that other brain factors triggered tau aggregation, we immunodepleted tau from the brain homogenates, which abolished all FRET signal (Fig. S3*B*).

Comparison of Seeding with Standard Histopathological Markers. Histopathological analysis has been widely used to quantify tau deposition and is currently the gold standard for postmortem diagnosis of AD and the related tauopathies (41, 42). Numerous monoclonal antibodies and dyes enable detection of tau in multiple forms and phosphorylation states. To test the relative utility of the biosensor assay for early detection of pathology, we stained brain sections derived from the left hemisphere of the same mice used for seed detection. We quantified tau load with several commonly used antibodies and reagents.

The MC1 antibody recognizes amino acids on both the N terminus (amino acids 7–9) and within the repeat domain (amino acids 313–322) of tau, two epitopes that are simultaneously available when tau protein assumes a disease-associated conformation. MC1 has been reported to stain pathological conformers of tau earlier and with higher specificity than other common markers (43). Here, we used MC1 (kindly provided by Peter Davies, The Feinstein Institute for Medical Research, Manhasset, NY) to de-

tect the progressive accumulation of misfolded tau. Immunohistological staining of P301S brain sections revealed a general absence of MC1 positivity in young and nontransgenic mice, consistent with the reported lack of staining in Braak stage 0 human subjects (43). At 3 mo, however, most mice displayed weak and diffuse MC1 positivity throughout the cortex and hippocampus, which became progressively more intense and widespread in both cell bodies and the neuropil by 6 and 9 mo (Fig. 6*A*). Strong cell body and neuropil staining manifested in both the cortex (Fig. 6*B*) and hippocampus (Fig. S4) beginning at 6 mo. Quantification of MC1 positivity, represented as the percent area of brain regions covered by positive MC1 staining, clearly demonstrated a corresponding trend in cortex (Fig. 6*C*) and hippocampus (Fig. 6*D*). Taking these data together, we conclude that MC1 reliably detects pathological tau beginning at 3 mo in these P301S mice.

The AT8 antibody recognizes tau protein that is phosphorylated at both serine 202 and threonine 205 residues (44). The antibody sensitively recognizes AD-derived tau and specifically recognizes hyperphosphorylated tau species (44), making it ideal for AD diagnostics. We used AT8 to detect progressive accumulation of hyperphosphorylated tau in our mouse cohort. Most brain sections lacked AT8 positivity until 6 mo, at which time it manifested in diffuse patterns throughout the neuropil. This signal increased in intensity with age (Fig. 7*A*). Higher magnification images showed slight cell body staining at 6 mo in the cortex (Fig. 7*B*) and hippocampus (Fig. S5), although intense and abundant neuronal cell body staining only became apparent at 9 mo. Quantification of AT8 positivity revealed substantial variation in 3- and 4-mo-old animals in both cortical (Fig. 7*C*) and hippocampal (Fig. 7*D*) regions. Some animals exhibited intense positivity whereas

A

B   AD   C   HD

D
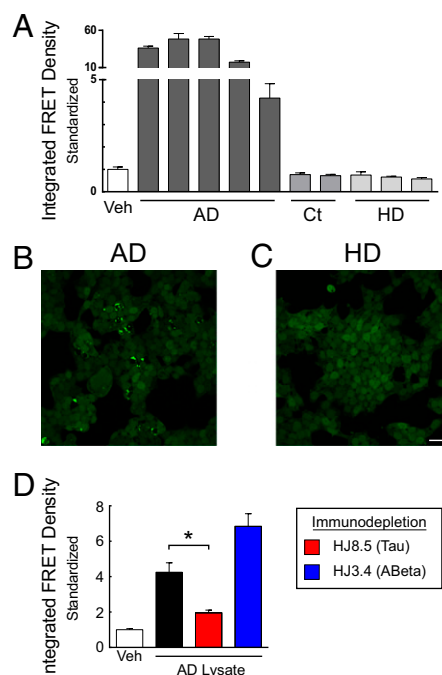
Fig. 4. Tau seeding activity is present in AD brains, but not aged, control brains, or HD brains. (*A*) Ten micrograms of clarified lysate [10% (wt/vol)] was transduced into HEK293T tau biosensor cells. After 24 h, cells were harvested for FRET flow cytometry. Tau seeding is detected in all AD brains and not in age-matched controls or HD brains. Confocal microscopy analysis of biosensor cells transduced with (*B*) AD or (*C*) HD brain homogenates. (Scale bar, 20 μM.) (*D*) Tau seeding activity is depleted with the anti-tau antibody, HJ8.5, but not the anti-Aβ antibody, HJ3.4. Error bars show SEM; $*P < 0.05$; one-way ANOVA.

Holmes et al.

Fig. 5. Seeding activity is present in the brains of P301S transgenic mice and increases with age. Microdissected brainstem (*A*), neocortex (*B*), frontal lobe (*C*), and hippocampus (*D*) from the right hemisphere were homogenized and 1.5 µL of clarifed lysate [10% (wt/vol)] was transduced into the tau biosensor cells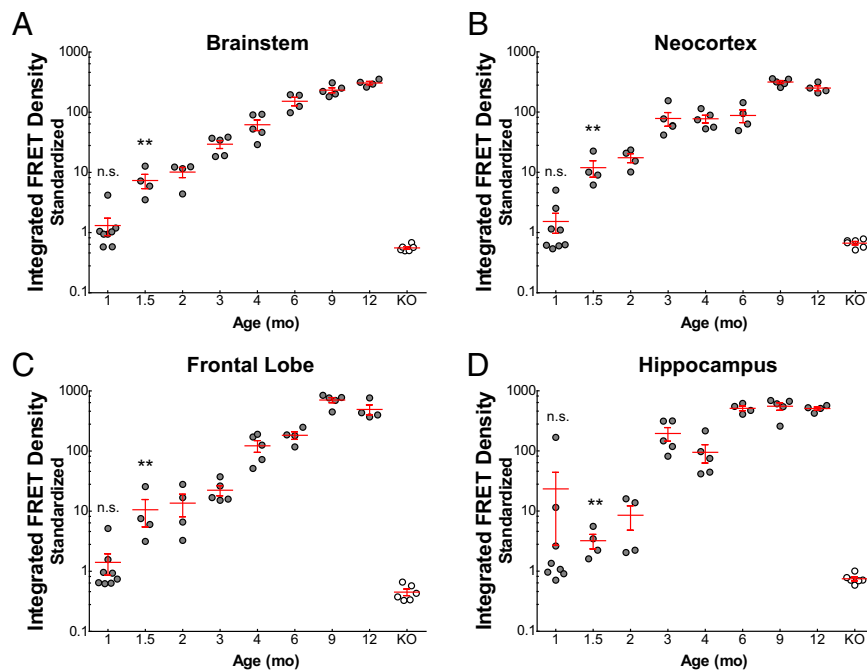. After 24 h, the biosensor cells were harvested for FRET flow cytometry. Tau seeding is detected in the P301S mouse line as early as 1.5 mo and increases with age. A minimum of four mice were analyzed per age group and all lysates were run in quadruplicate. Individual data points depict individual mice. Error bars show SEM; **P = 0.0004, Mann–Whitney U test, two-tailed exact significance; n.s., not significant.

others lacked it entirely. As previously reported (38), not until ~6 mo did AT8 reliably mark hyperphosphorylated tau accumulation.

To further compare markers of aberrantly folded tau (MC1) and hyperphosphorylated tau (AT8), we used a second phospho-tau antibody, PG5. PG5 recognizes phosphorlyated tau at serine 409 and marks neurofibrillary pathology in early and advanced AD, but not in normal brain tissue (45). PG5 staining in our P301S brain sections resulted in cell body and neuropil signal in both the cortex and hippocampus, starting at ~6 mo, and increased with age (Fig. S6 *A* and *B*). Quantification of PG5 re-activity revealed a similar trend with positivity commencing around 4–6 mo (Fig. S6 *C* and *D*), similar to that of AT8. Thus, markers of hyperphoshorylated tau (AT8 and PG5) succeed that of aberrantly folded tau (MC1) in our P301S cohort.

Thioflavin S (ThioS) fluoresces upon binding β-sheet structures, a biophysical property of protein amyloids (46). We stained brain sections of P301S mice with ThioS and found that signal was not apparent until 9 mo (Fig. S7*A*). To calculate ThioS positivity, we used a semiquantitative rank system (47). Quantification was largely consistent within cohorts and confirmed our initial impression that ThioS reliably detects amyloid deposits at 9 mo (Fig. S7 *B* and *C*).

In summary, we evaluated the onset and progression of pathological tau in brain sections from a large cohort of mice using four common histological markers. Conformationally aberrant tau (Fig. 6), hyperphosphorylated tau (Fig. 7 and Fig. S6), and amyloid deposits (Fig. S7) all tracked with age-dependent increases in pathology. However, the onset of reliable detection varied: MC1 (3 mo), AT8 and PG5 (6 mo), and ThioS (9 mo).

Tau Seeding Is the Earliest Marker of Pathology. To directly compare the timelines of seeding activity and immunohistochemical markers, we standardized each age cohort within a given parameter to a percent of its maximal burden (i.e., 100%) (Fig. 8*A*). We used nonlinear regression to fit the curves. The percentage

signal (S) S_{10} and S_{50} values were calculated to show the ages, represented in weeks, at which detection could be observed for each parameter. Standardization confirmed that seeding activity is the earliest marker of tau pathology, preceding the other histological markers by at least 4 wk (Fig. 8*A*). Finally, increases in tau seeding correlate well with histopathological stains, indicating that seeding activity reliably marks disease progression (Fig. 8*B*).

Discussion

Accumulating evidence implicates transcellular propagation of tau protein aggregates, or seeds, as a mechanism for disease progression in tauopathies. However, the extent to which seeding activity drives pathogenesis remains unknown. It is unclear whether seeding activity underlies progression of neurodegeneration, or is instead a consequence, or even mere epiphenomenon. To help address this question, we created a biosensor cell line to sensitively detect tau seeding activity in biological material. Using a within-animal approach, we compared the onset and progression of seeding activity versus common histological markers of tau in the P301S mouse model. We detected tau seeding activity >4 wk sooner than the best available histological marker (MC1). Furthermore, seeding activity quantifiably tracks disease progression. The early appearance and robust development of seeding activity are consistent with the hypothesis that tau seeds underlie disease progression, or are at least its most proximal marker.

FRET Flow Cytometry for Seed Detection. Most proteopathic seeding assays are based on the propensity of misfolded proteins to shorten the lag phase of amyloid formation, thus promoting nucleation and fibril growth. These assays have previously required the use of dyes (e.g., Thioflavin) that exhibit enhanced fluorescence when bound to β-sheet–rich structures. This approach has been used to monitor the seeding activity of prion protein (PrP), β-amyloid, huntingtin, and, most recently, tau seeds (48–52). Practically, these kinetic assays are arduous, requiring highly
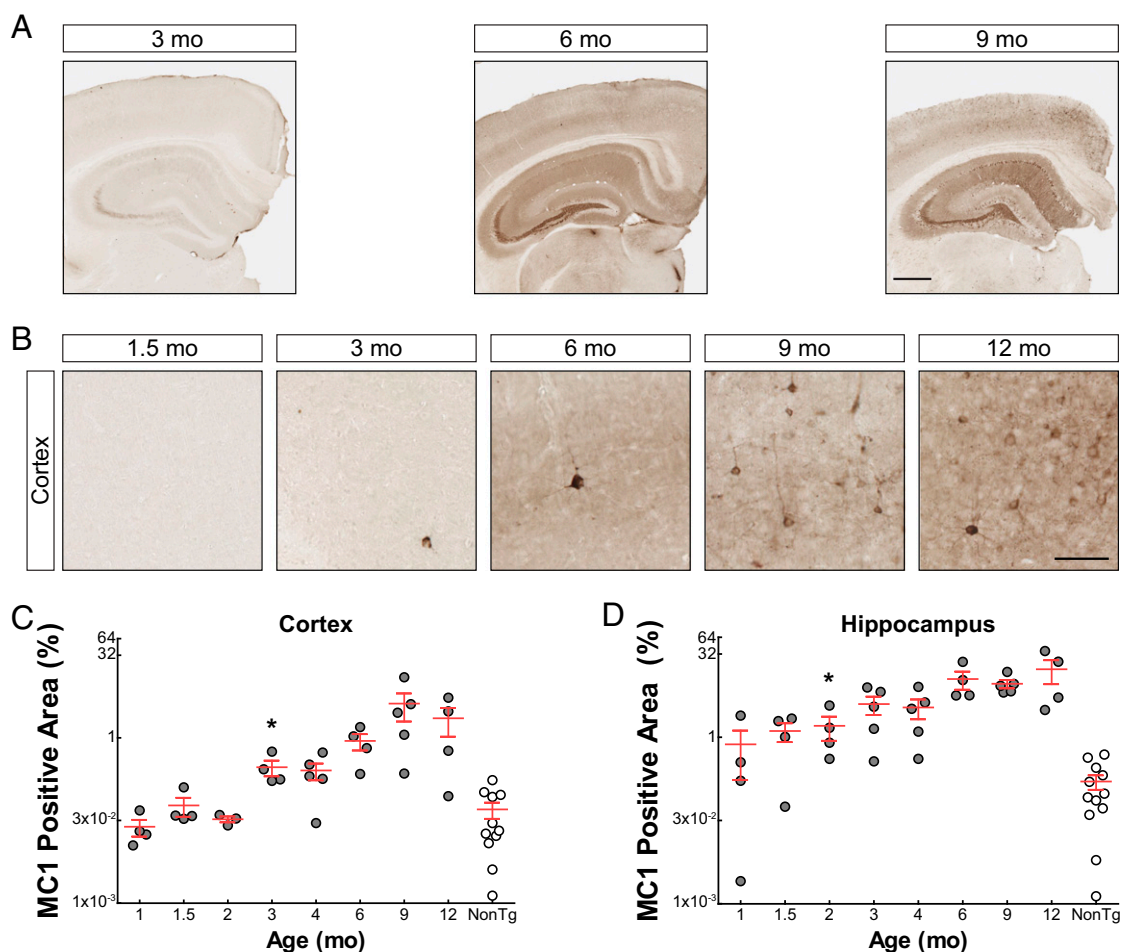
www.manaraa.com

Fig. 6. MC1 staining shows aberrant tau deposition at 3 mo. (*A*) Representative images from P301S transgenic animals at different ages, stained with MC1. (Scale bar, 0.5 mm.) (*B*) High-power images of the neocortex from the same brain sections shown in *A*. Weak staining can be seen in 3-mo-old animals, and stronger cell body staining can be seen in 6-mo-old animals. (Scale bar, 100 μm.) (*C* and *D*) Percent area covered by MC1 staining in the neocortex (*C*), and hippocampus (*D*). Note the age-dependent increase in MC1 signal for both regions. Error bars show SEM. Neocortex: *$P = 0.0074$; Hippocampus: *$P = 0.0091$; Mann–Whitney *U* test, two-tailed exact significance.

consistent preparation of purified recombinant protein substrates as well as the ability to maintain these substrates in the monomeric form. With the exception of PrP seed amplification, in vitro seeding assays for tau and related amyloids are relatively imprecise and generally insensitive to subnanomolar amounts of analyte (51, 52).

The biosensor cell seeding assay described here is quantitative, ultrasensitive, facile, and specific. We engineered a monoclonal HEK293T cell line to express tau RD-CFP and tau RD-YFP containing the P301S mutation. The P301S mutation in tau exhibits high sensitivity to seeding, yet doesn't readily aggregate on its own. Transduction of tau seeds from a variety of sources into the biosensor line triggers aggregation with a concomitant FRET response that is readily detected by flow cytometry. The assay detects recombinant wild-type tau RD seeds at 316 fM and has a dynamic range spanning three log orders-of-magnitude. The tau biosensor assay is specific to tau seeds, because heterologous amyloids, such as α-synuclein and huntingtin, do not trigger aggregation. Furthermore, only homotypic protein interactions produce FRET, because costimulation of synuclein-CFP and tau-YFP heterotypic biosensors leads to robust aggregation of both biosensor proteins, often within the same cellular inclusions, and does not produce a FRET signal. Although we cannot exclude a "FRET barrier" between synuclein-CFP and tau-YFP, it is likely

that tau and synuclein are not coassembling into the same filaments even though they partition into the same cellular locale.

Previous reports have suggested cross-seeding between synuclein and tau (53–55). Our laboratory has previously failed to demonstrate cross-seeding onto tau-expressing cells using fibrillar synuclein, amyloid β, or expanded huntingtin seeds (20). In this system, tau is fused to GFP variants that may inhibit crossseeding activity from heterologous amyloids. The data presented here aim only to test specificity of seeding onto the P301S tau biosensor line and not to establish a universal model for crossseeding studies. In the context of this assay, neither synuclein nor huntingtin seeds nucleated aggregation of tau, confirming the selectivity of the biosensor cell line for tau seeds and not generic amyloids.

We further validated this method in primary hippocampal neurons expressing tau RD-CFP/YFP biosensors. Even in the absence of liposome carriers we detected a dose-dependent increase in aggregation and FRET. Thus, although phospholipids increase seed detection efficiency in this system, they are not required. Importantly, we have also used this system to measure activity of other proteopathic seeds, including α-synuclein. We predict that this approach to monitor seeding can be reliably translated to many other protein amyloid disorders.

By generating a monoclonal FRET biosensor cell line, we have created a stable and infinitely amplifiable seed detection source
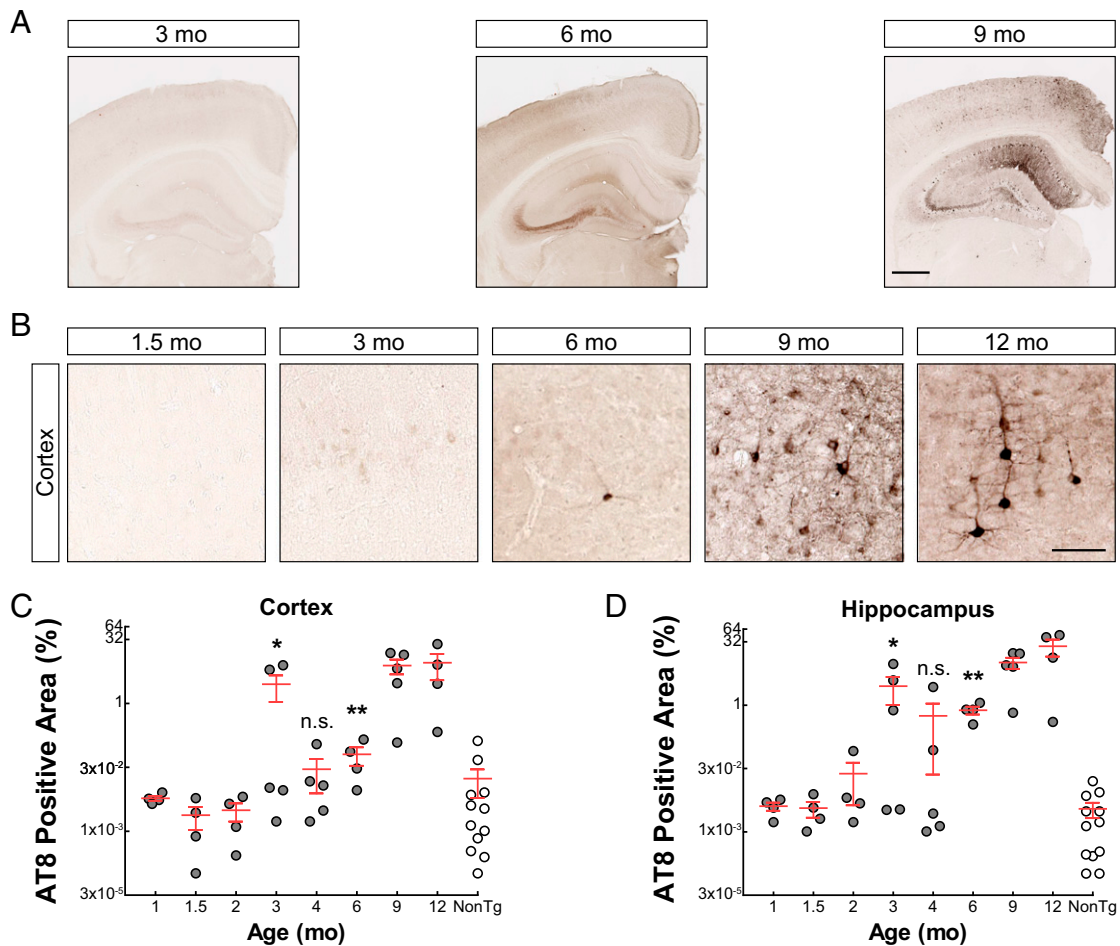
Fig. 7. AT8 staining shows phospho-tau deposition at 6 mo. (*A*) Representative images from P301S transgenic animals at different ages, stained with AT8. (Scale bar, 0.5 mm.) (*B*) High-power images of neocortex from the same brain sections shown in *A*. Cell body staining begins at 6 mo. (Scale bar, 100 µm.) (*C* and *D*) Percent area covered by AT8 staining of phospho-tau in the neocortex (*C*), and hippocampus (*D*). Note the age-dependent increase in AT8 signal for both regions with signal becoming reliably positive at 6 mo. Error bars show SEM. Neocortex: *$P = 0.040$, **$P = 0.025$; Hippocampus: *$P = 0.013$, **$P = 0.004$; Mann–Whitney U test, two-tailed exact significance.

that we have made available through a biological resource center (American Type Culture Collection). We empirically selected the most efficient FRET donor:acceptor ratio during the production of the cells. Because the biosensors are monoclonally derived, we have observed no drift in donor:acceptor ratios. Furthermore, flow cytometry has important advantages over other modes of FRET detection: we can monitor FRET at the population level (a feature of plate reader approaches) while maintaining single cell resolution (a feature of FRET microscopy). Development of the integrated FRET density metric allows highly quantitative and global assessment of aggregate burden within a cell population. Because this system is adaptable to FACS, we can reliably isolate and reculture cells as a function of FRET-associated aggregation states. This finding has important implications for cell-based genetic studies.

Tau Seeding Activity Is an Early Pathological Manifestation in a Tauopathy Mouse Model. Age-dependent changes in tau have been previously reported in the P301S mouse. In 2011, Yamada et al. (40) demonstrated with microdialysis that the ratio of monomeric ISF:CSF tau decreases with age. Additionally, we previously observed by biochemical extraction techniques that soluble total tau protein decreases with a concomitant increase in insoluble tau by 6–9 mo (40). Because of the late onset of solubility changes, the difficulty in precise quantification, and the very early appearance

of seeding activity, we did not monitor soluble versus insoluble tau levels in this study.

We used the seeding assay to determine the onset and progression of seeding activity in the P301S transgenic mouse, a model of tauopathy. We reasoned that if tau seeding is a critical component of disease pathogenesis, then activity should manifest early and increase over time. The P301S model has well-characterized disease-associated changes including neurofibrillary tangles, tau hyperphosphorylation, and behavior deficits (38, 39). To precisely determine the kinetics of seeding, we tested multiple brain regions from mice ranging in age from 1 to 12 mo. We reliably detected tau seeding activity at 1.5 mo, far in advance of any changes in histopathology. Seeding activity increased age-dependently, with brainstem showing the most consistent trends and hippocampus showing more variability.

P301S mice undergo numerous pathological manifestations with age, including gliosis, and synapse/neuron loss (38, 39). Although these features are important markers of disease, they represent generic changes that occur with numerous neurodegenerative disorders, and are not tauopathy-specific. Here, we developed a tau-specific seeding assay and compared these seeding results to histopathological markers of tau deposition, the current gold-standard technique for postmortem analysis of AD.

MC1 is reported as one of the earliest markers of misfolded tau protein (43, 56). In our study, MC1 indeed reliably marked
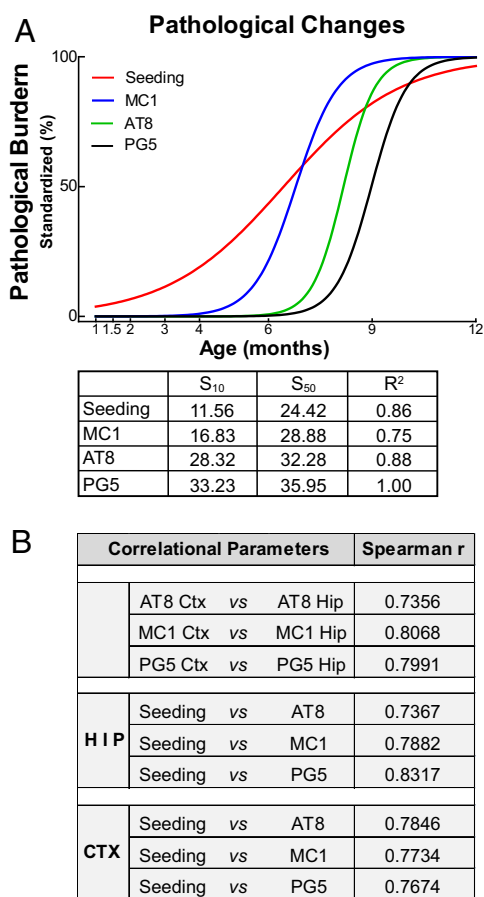
www.manaraa.com

A

Pathological Changes

	S_{10}	S_{50}	R^2
Seeding	11.56	24.42	0.86
MC1	16.83	28.88	0.75
AT8	28.32	32.28	0.88
PG5	33.23	35.95	1.00

B

Correlational Parameters			Spearman r
	AT8 Ctx	vs AT8 Hip	0.7356
	MC1 Ctx	vs MC1 Hip	0.8068
	PG5 Ctx	vs PG5 Hip	0.7991
HIP	Seeding	vs AT8	0.7367
	Seeding	vs MC1	0.7882
	Seeding	vs PG5	0.8317
CTX	Seeding	vs AT8	0.7846
	Seeding	vs MC1	0.7734
	Seeding	vs PG5	0.7674

Fig. 8. Tau seeding activity precedes other markers of tauopathy. (*A*) Tau seeding, MC1, AT8, and PG5 timecourse data were modeled using nonlinear regression analysis. The S_{10} and S_{50} was calculated for each parameter, represented in weeks. Tau seeding precedes other histopathological markers by more than 4 wk. Thioflavin S was not included because of its nonscalar ranking system. (*B*) Correlation analysis was conducted between different brain regions using the same antibody and between seeding activity and staining within the same brain regions. Seeding activity correlates well with AT8, MC1, and PG5 staining.

aberrant tau at 3 mo throughout the hippocampus and cortex. AT8, perhaps one of the most common tau-detection antibodies presently used, binds hyperphosphorylated tau (44, 57, 58). Although AT8 serves as an excellent stain in late-stage human AD brain, we observed reliable immunohistological staining beginning at ~6 mo in P301S mice, >4 mo after the onset of seed detection, suggesting that seeding activity precedes accumulation of hyperphosphorylated tau at this epitope. PG5, another marker of hyperphosphorylated tau, showed a similar kinetic course to AT8. We used ThioS to specifically test for the presence of β-sheet–rich structures. This stain was expected to appear late, as fibril-rich neurofibrillary tangles are late stage hallmarks (59). Indeed, we observed ThioS positivity at 9 mo in P301S mice. We have thus performed a detailed and comprehensive assessment of neuropathology in the P301S mouse and demonstrate that tau seeding is a very early and robust marker of tauopathy.

Seeding as Therapeutic Endpoint. Neurodegenerative disease mouse models are commonly used for the in vivo evaluation of therapeutic interventions. As an early marker of pathologic changes, tau seeding may serve as an excellent disease-outcome measure for future drug studies. Theoretically, an intervention could commence at just 1 mo, before the onset of pathology, and animals

could be killed and assessed for seeding at any time after 1.5 mo. This experimental approach would substantially reduce housing-associated costs and turnaround time for preclinical trials.

Histology currently serves as a gold standard for postmortem AD diagnostics, and such methods are clearly reliable for trained neuropathologists. However, the seeding assay may overcome some of the limitations associated with standard histology. Notably, experimental setup is straightforward, requiring only a general knowledge of cell culture and flow cytometry. Data analysis is quick and highly quantitative, excluding the possibility of subjective interpretation. Results are highly reproducible, in part because of the use of a monoclonal biosensor cell line. Finally, once seed material is prepared, the turnaround time of an experiment, including data analysis, is only 3 d. As represented in Fig. 4, the seeding assay directly translates to human brain homogenates, where it reliably and specifically detects aberrant tau in AD, but not normal monomeric tau in HD and control brains. Given the ease, sensitivity, and applicability demonstrated by this assay, we propose that it might be an ideal supplement to current AD and other tauopathy-related postmortem diagnostics.

In summary, we have combined the specificity of a tau monoclonal biosensor cell line and the sensitivity of FRET flow cytometry to directly compare the onset and progression of disease pathology between seeding and histological deposition. We find that tau seeding increases in an age-dependent manner in P301S mice and that onset occurs over 4 wk before the earliest histological marker of tau deposition. We conclude tau seeding activity serves as an early and robust marker of tauopathy, consistent with a proximal role for tau seeds in pathogenesis.

Methods

Stable Cell Line Generation. HEK 293T cells were plated at a density of 150,000 cells per well in a 24-well dish. The following day, cells were transduced with CFP or YFP lentiviral constructs, as described in *SI Methods*. Cells were grown in virus-containing media for 72 h before expanding. From a 10-cm dish, cells were harvested with 0.05% trypsin, resuspended in flow cytometry buffer (HBSS plus 1% FBS and 1 mM EDTA), and subjected to FACS (Sony Biotechnology). Populations of CFP and YFP dual-positive cells with a CFP:YFP median fluorescent intensity (MFI) ratio of 1:3.7 (standardized to their relative brightness) were selected to yield a FRET donor:acceptor molar ratio of 1:1. CFP or YFP single-positive cells with an equivalent MFI to dual-positive cells were selected. Following FACS and expansion, single-positive cells were maintained and used as a polyclonal line. Dual-positive cells were used to generate monoclonal lines. Here, cells were plated sparsely in a 10-cm dish and allowed to expand for 10 d, at which time cloning cylinders (Bel-Art Products) were used to isolate single clones. All stable cell lines were amplified, frozen down, and stored in liquid nitrogen until use. The derived monoclonal biosensor cell lines were empirically tested for best FRET signal to noise, and the same monoclonal cell line was used for all experiments.

Liposome-Mediated Transduction of Tau Seeds. Stable cell lines were plated at a density of 35,000 cells per well in a 96-well plate. Eighteen hours later, at 60% confluency, cells were transduced with proteopathic seeds. Transduction complexes were made by combining [8.75 μL Opti-MEM (Gibco) +1.25 μL Lipofectamine 2000 (Invitrogen)] with [Opti-MEM + proteopathic seeds] for a total volume of 20 μL per well. Liposome preparations were incubated at room temperature for 20 min before adding to cells. Cells were incubated with transduction complexes for 24 h.

FRET Flow Cytometry. Cells were harvested with 0.05% trypsin and postfixed in 2% paraformaldehyde (Electron Microscopy Services) for 10 min, then resuspended in flow cytometry buffer. The MACSQuant VYB (Miltenyi) was used to perform FRET flow cytometry. To measure CFP and FRET, cells were excited with the 405 nm laser, and fluorescence was captured with a 405/50 nm and 525/50 nm filter, respectively. To measure YFP, cells were excited with a 488 laser and fluorescence was captured with a 525/50 nm filter. To quantify FRET, we used a gating strategy similar to that previously described (25). Briefly, CFP bleed-through into the YFP and FRET channels was compensated using MACSQuantify Software from Miltenyi Biotec. Because some YFP-only cells exhibit emission in the FRET channel, we introduced and

Holmes et al.

additional gate to exclude from analysis cells that exert a false-positive signal in the FRET channel (i.e., false FRET gate). Subsequently, we created a final bivariate plot of FRET vs. CFP and introduced a triangular gate to assess the number of FRET-positive cells (Fig. S1A). This FRET gate was adjusted to biosensor cells that received lipofectamine alone and are thus FRET-negative. This allows for direct visualization of sensitized acceptor emission arising from excitation of the CFP donor at 405 nm. The integrated FRET density, defined as the percentage of FRET-positive cells multiplied by the median fluorescence intensity of FRET-positive cells, was used for all analyses. For each experiment, 20,000 cells per replicate were analyzed and each condition was analyzed in quadruplicate. Data analysis was performed using FlowJo v10 software (Treestar).

Cross Seeding and Homotypic FRET. For cross-seeding experiments, the P301S tau biosensor cell line was treated with either recombinant wild-type tau RD seeds, recombinant wild-type synuclein seeds, or synthetic $Htt_{Exon1}(Q50)$ seeds (500 nM each). Cells were treated for 24 h and harvested for FRET flow cytometry. For homotypic FRET experiments, HEK293 cells were transiently transfected with tau-CFP and tau-YFP, syn-CFP and syn-YFP, or syn-CFP and tau-YFP. Twenty-four hours later, cells were transduced with a mixture of 100 nM tau fibrils plus 100 nM synuclein fibrils. Cells were treated for 24 h and either harvested for FRET flow cytometry or replated in microslides for confocal microscopy analysis.

Mouse Brain Homogenate Preparation. Microdissected brain regions were suspended in 10% (wt/vol) ice-cold TBS containing cOmplete protease inhibitors (Roche). Tissue was homogenized at 4 °C using a probe sonicator (Omni Sonic Ruptor 250) at 30% power, receiving 25 pulses. Lysates were centrifuged at $21,000 \times g$ for 15 min to remove cellular debris and large, insoluble material. Supernatants were aliquoted and stored at −80 °C until further use.

1. Seeley WW, Crawford RK, Zhou J, Miller BL, Greicius MD (2009) Neurodegenerative diseases target large-scale human brain networks. *Neuron* 62(1):42–52.
2. Zhou J, Gennatas ED, Kramer JH, Miller BL, Seeley WW (2012) Predicting regional neurodegeneration from the healthy brain functional connectome. *Neuron* 73(6):1216–1227.
3. Raj A, Kuceyeski A, Weiner M (2012) A network diffusion model of disease progression in dementia. *Neuron* 73(6):1204–1215.
4. Braak H, Braak E (1991) Neuropathological stageing of Alzheimer-related changes. *Acta Neuropathol* 82(4):239–259.
5. Braak H, Braak E (1995) Staging of Alzheimer's disease-related neurofibrillary changes. *Neurobiol Aging* 16(3):271–278, discussion 278–284.
6. Prusiner SB (1984) Some speculations about prions, amyloid, and Alzheimer's disease. *N Engl J Med* 310(10):661–663.
7. Prusiner SB (2001) Shattuck lecture—Neurodegenerative diseases and prions. *N Engl J Med* 344(20):1516–1526.
8. Frost B, Jacks RL, Diamond MI (2009) Propagation of tau misfolding from the outside to the inside of a cell. *J Biol Chem* 284(19):12845–12852.
9. Clavaguera F, et al. (2009) Transmission and spreading of tauopathy in transgenic mouse brain. *Nat Cell Biol* 11(7):909–913.
10. Guo JL, Lee VMY (2011) Seeding of normal Tau by pathological Tau conformers drives pathogenesis of Alzheimer-like tangles. *J Biol Chem* 286(17):15317–15331.
11. Liu L, et al. (2012) Trans-synaptic spread of tau pathology in vivo. *PLoS ONE* 7(2): e31302.
12. de Calignon A, et al. (2012) Propagation of tau pathology in a model of early Alzheimer's disease. *Neuron* 73(4):685–697.
13. Holmes BB, et al. (2013) Heparan sulfate proteoglycans mediate internalization and propagation of specific proteopathic seeds. *Proc Natl Acad Sci USA* 110(33): E3138–E3147.
14. Iba M, et al. (2013) Synthetic tau fibrils mediate transmission of neurofibrillary tangles in a transgenic mouse model of Alzheimer's-like tauopathy. *J Neurosci* 33(3):1024–1037.
15. Kim W, et al. (2010) Interneuronal transfer of human tau between Lamprey central neurons in situ. *J Alzheimers Dis* 19(2):647–664.
16. Wu JW, et al. (2013) Small misfolded Tau species are internalized via bulk endocytosis and anterogradely and retrogradely transported in neurons. *J Biol Chem* 288(3): 1856–1870.
17. Dujardin S, et al. (2014) Neuron-to-neuron wild-type Tau protein transfer through a trans-synaptic mechanism: relevance to sporadic tauopathies. *Acta Neuropathol Commun* 2(1):14.
18. Clavaguera F, et al. (2013) Brain homogenates from human tauopathies induce tau inclusions in mouse brain. *Proc Natl Acad Sci USA* 110(23):9535–9540.
19. Yamada K, et al. (2014) Neuronal activity regulates extracellular tau in vivo. *J Exp Med* 211(3):387–393.
20. Sanders DW, et al. (2014) Distinct tau prion strains propagate in cells and mice and define different tauopathies. *Neuron* 82(6):1271–1288.
21. Pollitt SK, et al. (2003) A rapid cellular FRET assay of polyglutamine aggregation identifies a novel inhibitor. *Neuron* 40(4):685–694.
22. Kfoury N, Holmes BB, Jiang H, Holtzman DM, Diamond MI (2012) Trans-cellular propagation of Tau aggregation by fibrillar species. *J Biol Chem* 287(23):19440–19451.
23. Wischik CM, et al. (1988) Structural characterization of the core of the paired helical filament of Alzheimer disease. *Proc Natl Acad Sci USA* 85(13):4884–4888.
24. Sperfeld AD, et al. (1999) FTDP-17: An early-onset phenotype with parkinsonism and epileptic seizures caused by a novel mutation. *Ann Neurol* 46(5):708–715.
25. Banning C, et al. (2010) A flow cytometry-based FRET assay to identify and analyse protein-protein interactions in living cells. *PLoS ONE* 5(2):e9344.
26. Michel CH, et al. (2014) Extracellular monomeric tau protein is sufficient to initiate the spread of tau protein pathology. *J Biol Chem* 289(2):956–967.
27. Luk KC, et al. (2009) Exogenous alpha-synuclein fibrils seed the formation of Lewy body-like intracellular inclusions in cultured cells. *Proc Natl Acad Sci USA* 106(47):20051–20056.
28. Volpicelli-Daley LA, et al. (2012) Prion-like acceleration of a synucleinopathy in a transgenic mouse model. *Neurobiol Aging* 33(9):2225–2228.
29. Mougenot AL, et al. (2011) Prion-like acceleration of a synucleinopathy in a transgenic mouse model. *Neurobiol Aging*.
30. Luk KC, et al. (2012) Pathological α-synuclein transmission initiates Parkinson-like neurodegeneration in nontransgenic mice. *Science* 338(6109):949–953.
31. Luk KC, et al. (2012) Intracerebral inoculation of pathological α-synuclein initiates a rapidly progressive neurodegenerative α-synucleinopathy in mice. *J Exp Med* 209(5): 975–986.
32. Polymeropoulos MH, et al. (1997) Mutation in the alpha-synuclein gene identified in families with Parkinson's disease. *Science* 276(5321):2045–2047.
33. Collinge J, Clarke AR (2007) A general model of prion strains and their pathogenicity. *Science* 318(5852):930–936.
34. Frost B, Diamond MI (2010) Prion-like mechanisms in neurodegenerative diseases. *Nat Rev Neurosci* 11(3):155–159.
35. Holmes BB, Diamond MI (2014) Prion-like Properties of tau protein: The importance of extracellular tau as a therapeutic target. *J Biol Chem* 289(29):19855–19861.
36. Vascellari S, et al. (2012) Prion seeding activities of mouse scrapie strains with divergent PrPSc protease sensitivities and amyloid plaque content using RT-QuIC and eQuIC. *PLoS ONE* 7(11):e48969.
37. Murayama Y, et al. (2014) Ultrasensitive detection of PrPSc in the cerebrospinal fluid and blood of macaques infected with bovine spongiform encephalopathy prion. *J Gen Virol*, 10.1099/vir.0.066225-0.
38. Yoshiyama Y, et al. (2007) Synapse loss and microglial activation precede tangles in a P301S tauopathy mouse model. *Neuron* 53(3):337–351.
39. Takeuchi H, et al. (2011) P301S mutant human tau transgenic mice manifest early symptoms of human tauopathies with dementia and altered sensorimotor gating. *PLoS ONE* 6(6):e21050.
40. Yamada K, et al. (2011) In vivo microdialysis reveals age-dependent decrease of brain interstitial fluid tau levels in P301S human tau transgenic mice. *J Neurosci* 31(37): 13110–13117.
41. Montine TJ, et al.; National Institute on Aging; Alzheimer's Association (2012) National Institute on Aging-Alzheimer's Association guidelines for the neuropathologic assessment of Alzheimer's disease: A practical approach. *Acta Neuropathol* 123(1):1–11.
42. Hyman BT, et al. (2012) National Institute on Aging-Alzheimer's Association guidelines for the neuropathologic assessment of Alzheimer's disease. *Alzheimers Dement* 8(1):1–13.
43. Weaver CL, Espinoza M, Kress Y, Davies P (2000) Conformational change as one of the earliest alterations of tau in Alzheimer's disease. *Neurobiol Aging* 21(5):719–727.
44. Biernat J, et al. (1992) The switch of tau protein to an Alzheimer-like state includes the phosphorylation of two serine-proline motifs upstream of the microtubule binding region. *EMBO J* 11(4):1593–1597.
45. Jicha GA, et al. (1999) cAMP-dependent protein kinase phosphorylations on tau in Alzheimer's disease. *J Neurosci* 19(17):7486–7494.
46. Santa-María I, Pérez M, Hernández F, Avila J, Moreno FJ (2006) Characteristics of the binding of Thioflavin S to tau paired helical filaments. *J Alzheimers Dis* 9(3): 279–285.
47. Yanamandra K, et al. (2013) Anti-tau antibodies that block tau aggregate seeding in vitro markedly decrease pathology and improve cognition in vivo. *Neuron* 80(2): 402–414.
48. Colby DW, et al. (2007) Prion detection by an amyloid seeding assay. *Proc Natl Acad Sci USA* 104(52):20914–20919.
49. Du D, et al. (2011) A kinetic aggregation assay allowing selective and sensitive amyloid-β quantification in cells and tissues. *Biochemistry* 50(10):1607–1617.

www.manaraa.com

50. Gupta S, Jie S, Colby DW (2012) Protein misfolding detected early in pathogenesis of transgenic mouse model of Huntington disease using amyloid seeding assay. *J Biol Chem* 287(13):9982–9989.

51. Morozova OA, March ZM, Robinson AS, Colby DW (2013) Conformational features of tau fibrils from Alzheimer's disease brain are faithfully propagated by unmodified recombinant protein. *Biochemistry* 52(40):6960–6967.

52. Salvadores N, Shahnawaz M, Scarpini E, Tagliavini F, Soto C (2014) Detection of misfolded A2 oligomers for sensitive biochemical diagnosis of Alzheimer s disease. *Cell Rep* 7(1):261–268.

53. Giasson BI, et al. (2003) Initiation and synergistic fibrillization of tau and alpha-synuclein. *Science* 300(5619):636–640.

54. Kotzbauer PT, et al. (2004) Fibrillization of alpha-synuclein and tau in familial Parkinson's disease caused by the A53T alpha-synuclein mutation. *Exp Neurol* 187(2):279–288.

55. Guo JL, et al. (2013) Distinct α-synuclein strains differentially promote tau inclusions in neurons. *Cell* 154(1):103–117.

56. Haroutunian V, Davies P, Vianna C, Buxbaum JD, Purohit DP (2007) Tau protein abnormalities associated with the progression of Alzheimer disease type dementia. *Neurobiol Aging* 28(1):1–7.

57. Goedert M, Jakes R, Vanmechelen E (1995) Monoclonal antibody AT8 recognises tau protein phosphorylated at both serine 202 and threonine 205. *Neurosci Lett* 189(3):167–169.

58. Braak H, Alafuzoff I, Arzberger T, Kretzschmar H, Del Tredici K (2006) Staging of Alzheimer disease-associated neurofibrillary pathology using paraffin sections and immunocytochemistry. *Acta Neuropathol* 112(4):389–404.

59. Arnold SE, Hyman BT, Flory J, Damasio AR, Van Hoesen GW (1991) The topographical and neuroanatomical distribution of neurofibrillary tangles and neuritic plaques in the cerebral cortex of patients with Alzheimer's disease. *Cereb Cortex* 1(1):103–116.

NEUROSCIENCE

Holmes et al.

www.manaraa.com